Nanoscale

Selective Desolvation in Two-Step Nucleation Mechanism Steers Crystal Structure Formation

Journal:	*Nanoscale*
Manuscript ID	NR-ART-09-2021-006346.R1
Article Type:	Paper
Date Submitted by the Author:	03-Dec-2021
Complete List of Authors:	Dighe, Anish; University of Illinois at Chicago, Chemical Engineering Coliaie, Paria; University of Illinois at Chicago, Department of Chemical Engineering Podupu, Prem; University of Illinois at Chicago, Chemical Engineering Singh, Meenesh; University of Illinois at Chicago, Chemical Engineering

Selective Desolvation in Two-Step Nucleation Mechanism Steers Crystal Structure Formation

Anish V. Dighe, Paria Coliaie, Prem K.R. Podupu, Meenesh R. Singh*

Department of Chemical Engineering, University of Illinois at Chicago, Chicago, IL 60607, United States

Corresponding Author:
Prof. Meenesh R. Singh
Assistant Professor
Department of Chemical Engineering
929 W. Taylor St
University of Illinois at Chicago
Chicago, IL 60607
Tel: (312) 996-3424
Email: mrsingh@uic.edu

Keywords: Two-Step Nucleation, Selective Desolvation, Crystal Structure Prediction, Molecular Dynamics, Sequential Desolvation

Abstract:
The two-step nucleation (TSN) theory and crystal structure prediction (CSP) techniques are two disjointed yet popular methods to predict nucleation rate and crystal structure, respectively. The TSN theory is a well-established mechanism to describe the nucleation of a wide range of crystalline materials in different solvents. However, it has never been expanded to predict the crystal structure or polymorphism. On the contrary, the existing CSP techniques only empirically account for the solvent effects. As a result, the TSN theory and CSP techniques continue to evolve as separate methods to predict two essential attributes of nucleation – rate and structure. Here we bridge this gap and show for the first time how a crystal structure is formed within the framework of TSN theory. A sequential desolvation mechanism is proposed in TSN, where the first step involves partial desolvation to form dense clusters followed by selective desolvation of functional groups directing the formation of crystal structure. We investigate the effect of the specific interaction on the degree of solvation around different functional groups of glutamic acid molecules using molecular simulations. The simulated energy landscape and activation barriers at increasing supersaturations suggest sequential and selective desolvation. We validate computationally and experimentally that the crystal structure formation and polymorph selection is due to a previously unrecognized consequence of supersaturation-driven asymmetric desolvation of molecules.

1. Introduction

Two-step nucleation is a well-established mechanism for a wide range of crystalline materials.(1) It has been validated experimentally and computationally.(2-4) In this mechanism, solute molecules in the solution are partially desolvated to form locally dense liquid clusters followed by complete desolvation to yield crystalline solids. The energy and lifetime of the dense liquid clusters determine the rate of nucleation. The two-step nucleation theory has successfully estimated nucleation rates for several crystalline materials better than the single-step classical nucleation theory.(5) The two-step nucleation theory starts from the premise that solute molecules undergo sequential desolvation to form denser structures. However, the process of self-assembly of molecules towards a particular crystal structure in these dense liquid clusters has remained elusive. Here we show partial desolvation of solute molecules forms dense liquid clusters, wherein molecules desolvates selectively based on the interactions of functional groups with solvents to form a crystal structure.

Traditionally, the solvation dynamics are studied with respect to the relaxation time of solvent molecules around a solute molecule.(6) The solvent molecules in the solvation shell behave differently to a change in solvent environment than the solvent molecules in bulk.(7) Many experimental and computational studies of solvation dynamics aimed to obtain the solvation time correlation function (STCF). It describes the response of solvent molecules in the solvation shell to an ultrashort high-energy pulse.(7-10) The pulse causes the excitation of solute molecules and, in turn, changes the configuration of solvent molecules in the solvation shell. Such solvation dynamics of many solvents around various complex solute molecules have been reported in the literature, and water molecules are known to have the fastest solvation dynamics.(11-13) More recently, the solvation shell dynamics are studied to understand the role of solvent molecules in the self-assembly of different classes of materials. In the case of ion transport in electrolytic solutions, the thickness of the solvation shell affects the mobility of ions and their stacking in the electric double layer, which in turn impacts the performance of the electrochemical cell.(14) For biomolecules such as proteins, the extent of hydration impacts the configuration of protein molecules which is responsible for their activity.(15, 16) In the case of crystallization, which is the focus of this work, the solvent molecules near the solute molecules affect the minimum energy path taken by a solute molecule in bulk to integrate into a kink site of a growing crystal.(17) However, none of the studies have developed a full mechanistic understanding of dynamics of desolvation involved in the process of nucleation of organic molecules. A quantitative explanation to the effect of sequential desolvation on the crystal structure formation is necessary to predict nucleation.

The theoretical approaches used to understand crystallization are primarily focused on the determination of nucleation and growth rates.(18, 19) The role of solvation shell dynamics in nucleation and growth rate theories is not explicitly considered, except for very few cases.(17, 20) Mostly, the solvation effects are included empirically in these rate calculations. In these approaches, the formation of the crystal structure is not specifically included, and these are typically considered separately using a different type of computational approach referred to as

crystal structure prediction (CSP) techniques. The CSP techniques involve calculating lattice energies assuming that the crystal structures with the lowest lattice energies are preferred experimentally.(21) Such approaches are aimed at understanding the polymorphism in the organic crystals. However, the hypothesis that the crystal structure with the lowest lattice energy will be the experimentally observed crystal structure is not valid for many organic molecules.(22, 23) To correctly predict polymorphism, it is necessary to consider both: the energetics of packing of molecules in the lattice and the solute-solvent interactions during crystallization. The latter part is not captured in the calculation of lattice energies. Recently, lattice energy calculations are evolved to capture the solvent effects while exploring the crystal energy landscape. The presence of solvent molecules during the exploration crystal energy landscape has instead resulted in predicting theoretical crystal structures near local energy minima with solvent molecules trapped inside the crystal lattice.(24)

A two-step nucleation mechanism with glutamic acid molecule as the solute and water as the solvent is shown in **Figure 1**. As soon as the solute molecules are dissolved in a solvent, the solvation shells are formed where the local density of the solvent molecules is higher than the bulk (see **Figure 1a**). This solvation shell must be fully depleted for crystallization to occur.(17) The depletion of the solvation shell is facilitated by increasing supersaturation. Supersaturation is achieved by either: (i) using an anti-solvent to reduce the solubility of the solute molecules in the solution, (ii) cooling the solution to reduce the solubility of solute, or (iii) evaporating the excess solvent. The increased interactions of solute in supersaturated solution causes partial desolvation of solute, which is the transition state for the first step of the two-step mechanism (see **Figure 1b**). The solute molecules in this transition state can relax to form a metastable state of a denser liquid cluster (see **Figure 1c**). Based on the stability of this dense liquid cluster, it can either lead to liquid-liquid phase separation (LLPS) or complete desolvation to form ordered crystalline material (see **Figure 1d**). An illustration of the energy profile for the two-step nucleation is shown in the inset. It is apparent that the sequential desolvation dynamics are closely related to the crystal structure formation. Such detailed considerations are necessary to predict crystal structure formation during nucleation.

In this article, we apply molecular simulation techniques to identify sequential desolvation dynamics in a supersaturated solution of glutamic acid molecules in water. The objective here is to map the solvation dynamics to the formation of either of the two polymorphs of glutamic acid crystals. The two polymorphs of glutamic acid crystals are (1) metastable- α polymorph and (2) stable- β polymorph. The distribution of water molecules around three functional groups of glutamic acid molecules points to the asymmetry of the solvation shell due to functional group-specific interactions of the solute molecule. The three functional groups are (a) carboxylate (COO^-), (b) quaternary amine (NH_3^+), and (c) carboxylic acid (COOH). The asymmetry of the solvation shell is then visualized using spatial distribution functions (SDFs). The partially desolvated structure is used to obtain an interaction energy landscape to relate energy minima to the crystal

structure. The results obtained from the energy landscape are then validated using batch crystallization experiments as well as the Umbrella sampling technique.

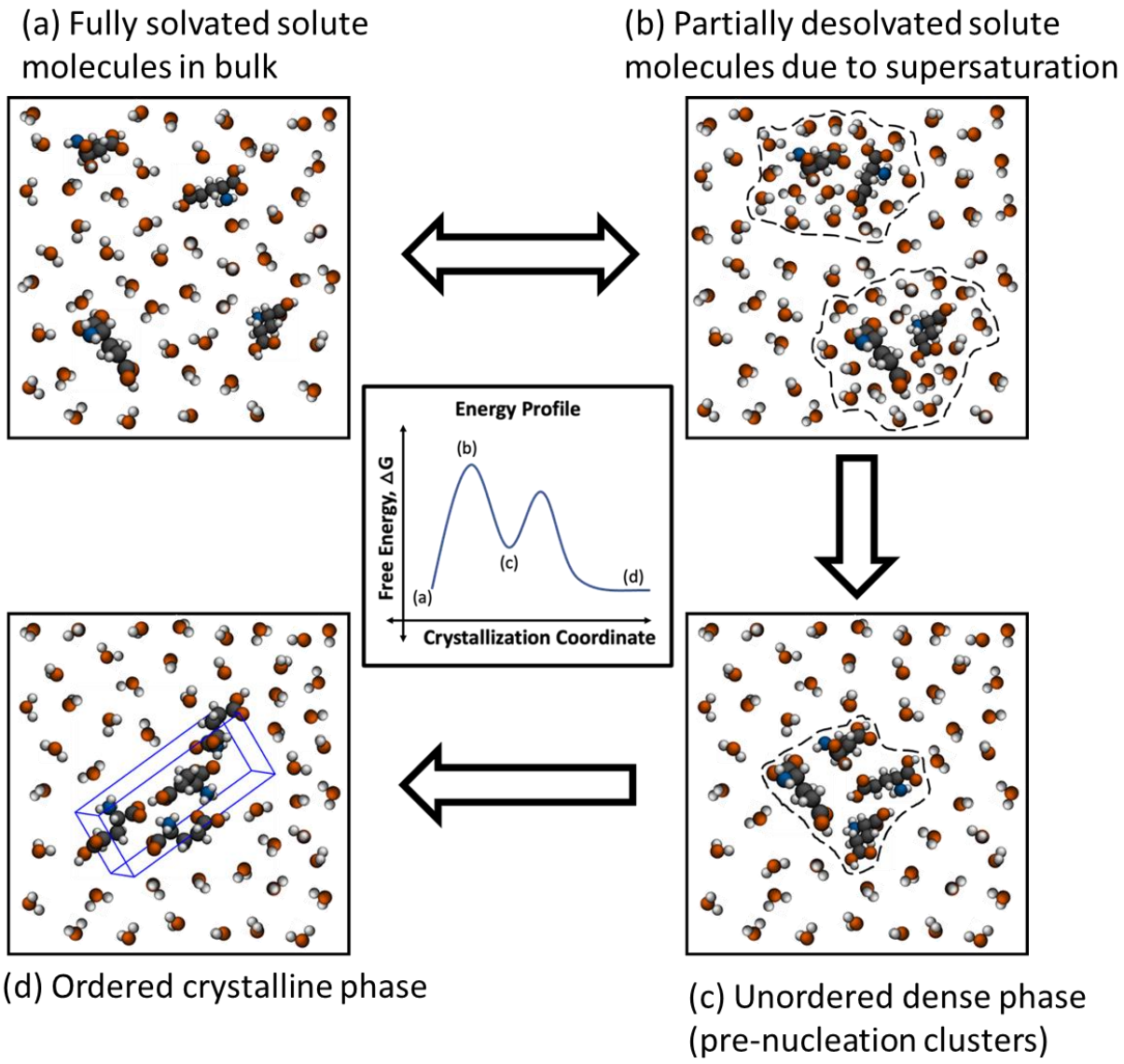

Figure 1: A pictorial representation of a two-step nucleation mechanism for glutamic acid molecule in water. (a) The glutamic acid molecules dissolved in bulk with a full solvation shell. (b) The first transition state of partially desolvated glutamic acid molecules is due to higher intermolecular interactions at increased supersaturation. (c) Aggregation of partially desolvated molecules to form a metastable, dense liquid cluster. (d) The unordered molecules in the dense liquid cluster can either grow to form an oiled-out state or order into a crystalline phase. The transition of the dense liquid cluster to the crystalline phase is the second step of nucleation which determines the crystal structure. The inset shows an illustration of a free energy diagram with states (a), (b), (c), and (d) marked in the profile.

2. Results and Discussion

Sequential desolvation of glutamic acid (GLU) molecules in aqueous solution at increasing supersaturation were investigated using molecular dynamics (MD) simulations with an objective to obtain mechanistic insights into crystal structure formation. Initially, the distribution functions were used to understand the distribution of water molecules around the GLUs, and then further analysis was performed to understand crystal structure formation. The protocol followed in this article is summarized in **Figure S1** of the supporting information (SI). The simulation details and force field validation details are given in **Section S1**, and **Figures S2 – S5** of SI.

Figure 2 shows the radial distribution functions (RDFs) of water molecules around different functional groups of interacting GLUs at two different supersaturation ratios of $\sigma = 1.2$ (low) and $\sigma = 2.5$ (high). The relative distances were tracked to identify interacting GLUs in the simulation box, and the portions of the MD trajectories where the distance between two GLUs is less than twice the solvation shell thickness (i.e. 1.2 nm) were shortlisted (refer to **Sections S2.1 – S2.2** of the SI). The average solvation shell thickness of the glutamic acid molecules is around 0.6 nm.(25) Such molecule pairs are significantly interacting because of the depletion of solvent molecules around them. For all such portions of MD trajectories, the RDFs of oxygen atom on the water molecule around: (i) carbon atom on COO^- functional group, (ii) nitrogen atom on NH_3^+ functional group, and (iii) carbon atom on the COOH functional group were calculated. The peak of the RDF denotes the highest local density of the water molecules at a specific distance. The first minima indicate the thickness of the primary solvation shell. In **Figures 2a-2c**, any two curves with identical locations of minima represent the same functional group on the two interacting GLUs at different supersaturation. **Figure 2a** shows the distribution of the water molecules around the COO^- functional groups of two interacting GLUs. **Figures 2b and 2c** show the water distribution around functional groups during stronger interaction of NH_3^+ - COO^-, and NH_3^+ - NH_3^+ functional groups, respectively. In **Figure 2a**, the curves showing the RDF of water at low and high supersaturations overlap, indicating the symmetric distribution of water molecules around the two functional groups. However, in **Figure 2b**, NH_3^+ functional group has a higher peak than the COO^- functional group at both supersaturation ratios, indicating the asymmetric distribution of water molecules during such interaction. Furthermore, the lower thickness of the solvation shell and the higher peak of the NH_3^+ functional group indicate a high affinity of water molecules towards the NH_3^+. At high supersaturation, the density of water molecules around both functional groups is significantly reduced. This is due to higher interactions between GLU. **Figure 2c** shows that both molecules have a significant number of water molecules around the NH_3^+ functional group. However, at higher supersaturation, the NH_3^+ of GLU #2 desolvates more than GLU #1. The RDFs of COOH functional groups are given in the **Figure S6** of the SI. The peak height of the COOH functional group is almost always near to the value of one, indicating that local solvation shell density around the functional group is equal to the bulk density of the water molecules. Hence, the desolvation of the COOH functional group can readily occur than the other functional groups. **Figure 2d** shows the different layers of the solvation shell embedded into the

average solvation shell. The average RDF curve describes the distribution of water molecules around the center of mass of the glutamic acid molecule. The smaller solvation shell thickness of the functional group-specific RDFs shows that the average solvation shell has smaller subshells embedded into itself. Based on all the RDFs, it can be clearly said that the solvation shell around the GLU is highly asymmetric. Such asymmetric distribution arises strongly due to electrostatic interactions. Since the crystal structure of both polymorphs of GLU is devoid of water molecules,(26) all functional groups have to undergo desolvation before forming a crystal. Based on the stronger affinity of the water molecules towards the NH_3^+ functional group, it is expected that desolvation of the NH_3^+ functional group will contribute significantly towards the activation energy required to form a crystal structure.

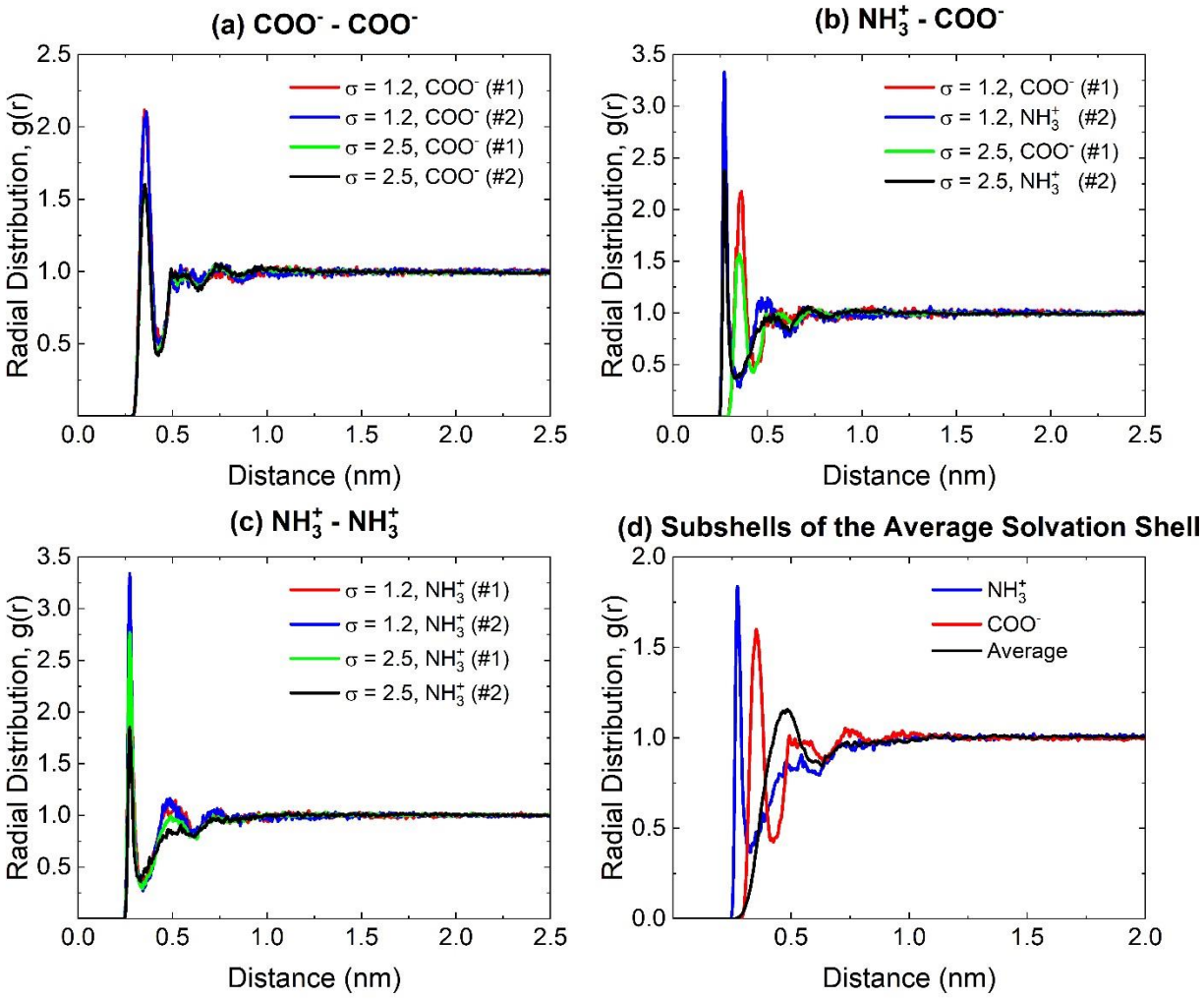

Figure 2: Radial distribution functions (RDFs) of water around glutamic acid molecule when two of the functional groups are strongly interacting- (a) COO^- - COO^- interaction, (b) NH_3^+ - COO^- interaction, and (c) NH_3^+ - NH_3^+ interaction. (d) Subshells of the average solvation shell at $\sigma = 2.5$. The average solvation shell is obtained by analyzing the oxygen atom around the center of mass of the glutamic acid molecule. The functional group-specific RDFs are embedded inside the

average solvation shell. In figures (a) – (c), the two curves representing the same supersaturation ratio are for two similar functional groups of the interacting GLUs (#1 and #2).

The asymmetric distribution of solvation shells around GLU is visualized using spatial distribution functions (SDFs) in **Figure 3** (refer to **Section S2.3** of the SI). **Figures 3a – 3c** show the reduction of the local density of water molecules around the functional group relative to the average solvation shell density of GLU, as shown in the **Figures S7 – S8** of the SI. The density of the water molecules in the solvation shell decreases in all functional group interactions with increasing supersaturation. The relative density near COO^- functional group during COO^- - COO^- (**Figure 3a**) and COO^- - NH_3^+ (**Figure 3b**) interaction nearly approaches the average shell density. However, the relative density near NH_3^+ (**Figure 3c**) functional group is significantly higher than the average shell density even at higher supersaturations. Such asymmetry in desolvation can be clearly seen in the SDFs plots shown in **Figure 3d – 3i**. SDF plots are generated to show the distribution of water around one of the interacting GLUs. The solid surface in the SDF plots shows the region around the GLU where the density of water molecules is 2.3 times the bulk density of water. The value of 2.3 is chosen based on the average peak heights of RDFs shown in **Figures 2a-2c**. At lower supersaturation, COO^- and NH_3^+ functional groups have a high density of water around them (**Figures 3d-3f**). However, the alkane chain and the COOH functional groups are highly desolvated. At higher supersaturation, the entire GLU is desolvated except for the NH_3^+ functional group that retains its solvation shell (**Figure 3g-3i**). The high affinity of water molecules towards of NH_3^+ functional group prevents desolvation of the GLU molecule at higher supersaturation. However, higher supersaturation also completely exposes the partially charged COO^- functional group during the interaction of GLUs. The possibility of strong repulsive interactions between COO^- functional groups raises the question of whether such interaction affects the minimum in the crystal energy landscape.

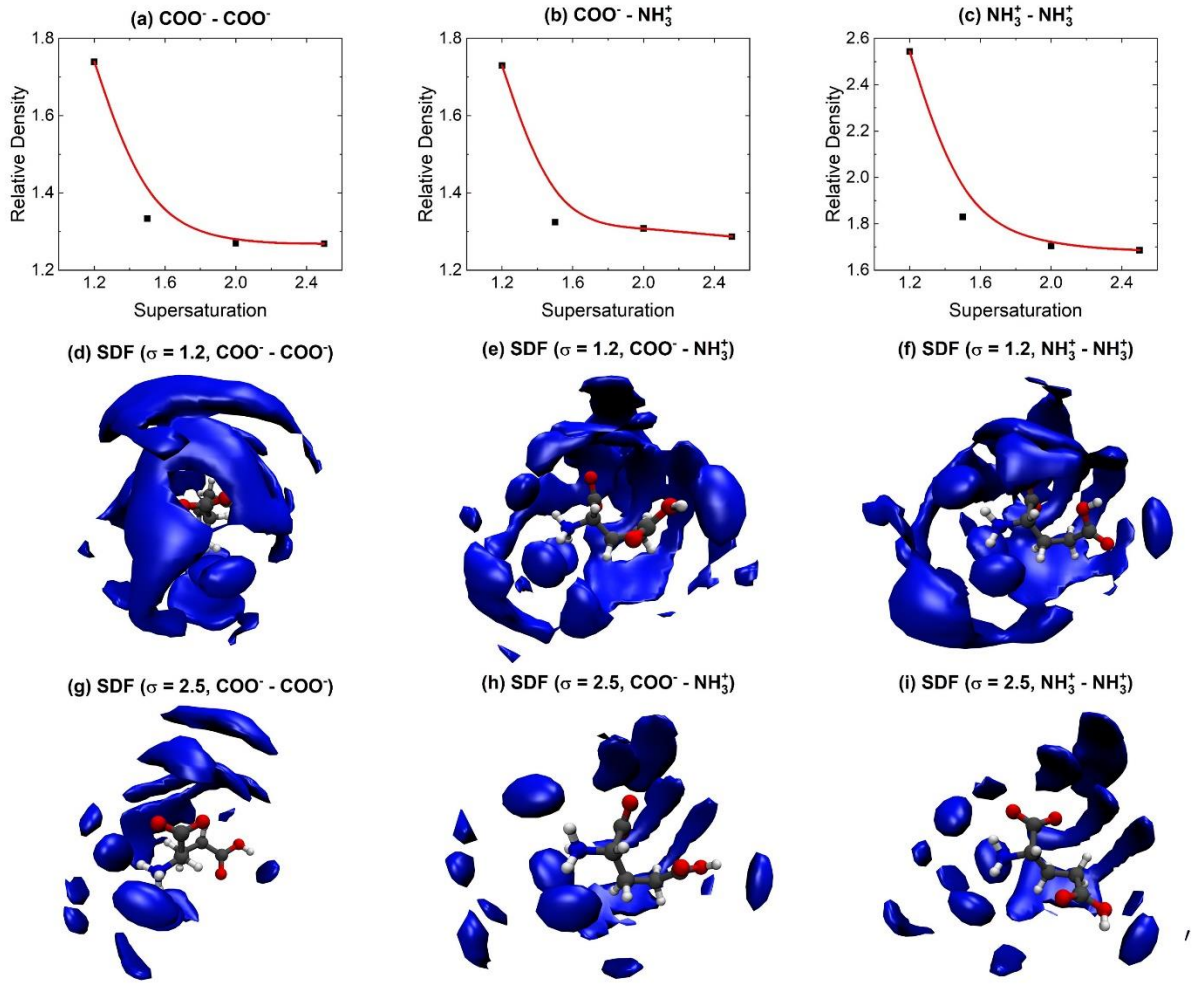

Figure 3: Variation in the local density of water molecules relative to the average solvation shell density during the interaction of the two functional groups (a) COO^--COO^-, (b) COO^-—NH_3^+, and (c) NH_3^+-NH_3^+ as a function of supersaturation. The spatial distribution functions (SDFs) of one of the interacting GLUs during (d) COO^--COO^-, (e) COO^--NH_3^+, and (f) NH_3^+-NH_3^+ interactions at lower supersaturation. SDFs of one of the interacting GLUs during (g) COO^--COO^-, (h) COO^-—NH_3^+, and (i) NH_3^+-NH_3^+ interactions at higher supersaturation.

Figure 4 shows the interaction energy landscape (potential of mean force) of the two interacting GLUs at low and high supersaturations (refer to **Sections S2.4 and S2.5** of the SI) and validates the polymorph selection using the Umbrella sampling technique (refer to **Section S3** of the SI). The energy landscape is obtained to find the lowest energy configuration of the interacting GLUs after the transition state (partially desolvated state, see **Figure 1b**) has been reached. The transition state of molecules is calculated using a previously-established double-well potential approach.(25, 27) The configuration of the two GLUs at the transition point was obtained from MD simulation. Next, they were rotated individually in a complete circle around the x-, y-, and z-axes using rotation matrices. The interaction energy at each rotation interval was calculated using

the intermolecular potentials obtained from the OPLS-AA forcefield. These rotations capture various relative configurations that GLUs can take in an unordered dense phase (see **Figure 1c**). **Figure 4a** shows the energies of these configurations, which are specified as a relative distance between α and γ carbon atoms of GLU #1 and #2. To further decide which configurations in the unordered state favors specific polymorphs of GLU crystals, the relative orientations of GLU molecules in the lattice of α and β polymorphs were analyzed. Next, the regions of relative orientations that have the most resemblance to α and β polymorphs were identified. **Figure 4a** shows the β region envelops the global minimum configuration at lower supersaturation. However, at higher supersaturation (**Figure 4b**), the global minimum is enclosed by the α region. These configurations at global minimum are favorable energetically in an unordered dense phase. It is more likely that these configurations will lead to respective crystal structures in the enclosed regions.

The Umbrella sampling technique was implemented to calculate the activation barriers to validate the crystal structures estimated from the potential of the mean force approach shown in **Figures 4a and 4b**. **Figures 4c and 4d** show the activation barriers for the formation of the α and β polymorphs obtained from the umbrella sampling technique at the supersaturation ratios of 1.2 and 2.5, respectively. The pull force profiles obtained during the steered MD simulation, and the number of samples at each distance are shown in **Figures S9 and S10** of SI, respectively. The solid black curves in **Figures 4c and 4d** show the activation barrier for the first step of two-step nucleation theory, which involves partial desolvation of GLU. This activation barrier has been previously benchmarked and validated for GLU.(25) The first peak in **Figures 4c and 4d** is associated with desolvation of secondary and tertiary solvation shells, whereas the second peak corresponds to desolvation of primary shell which are specific to functional group interactions. The red and blue curves represent the energy profiles obtained by performing the umbrella sampling simulations using the starting molecular configuration obtained from the crystal structures of α and β polymorphs. The highlighted region of the group specific interaction is obtained by analyzing the distances between center of mass of the interacting GLUs during the group specific interactions, as shown in **Figure S11** of the SI. The second activation barrier, which arises after the initial activation barrier in the energy profile of the α polymorph at $\sigma = 1.2$, and of the β polymorph at $\sigma = 2.5$, indicate that these polymorphs are less likely to be crystallized at the corresponding supersaturations. These observations are consistent with the interaction energy landscapes shown in **Figures 4a and 4b**. The first step of partial desolvation followed by the second step of selective desolvation constitutes the two-step nucleation mechanism, which steers the formation of a specific crystal structure. The activation barrier energy profile for $\sigma = 2$ is shown in the **Figure S12** of the SI.

The interaction energy landscapes before and at the transition state were compared to confirm that the location of the global minimum is not due to fluctuations in MD simulations. The two energy landscapes are shown in the **Figure S13** of the SI. The blue line connecting the two landscapes clarifies the positions of points of global energy minimum. The point at which the global minimum occurs at the transition state is not the global minimum in the pre-transition state

configuration. Indicating that such configuration may not be seen in the MD simulations since it has higher interaction energy. It also further validates that an activation barrier must be crossed for a specific configuration to appear at the global energy minimum.

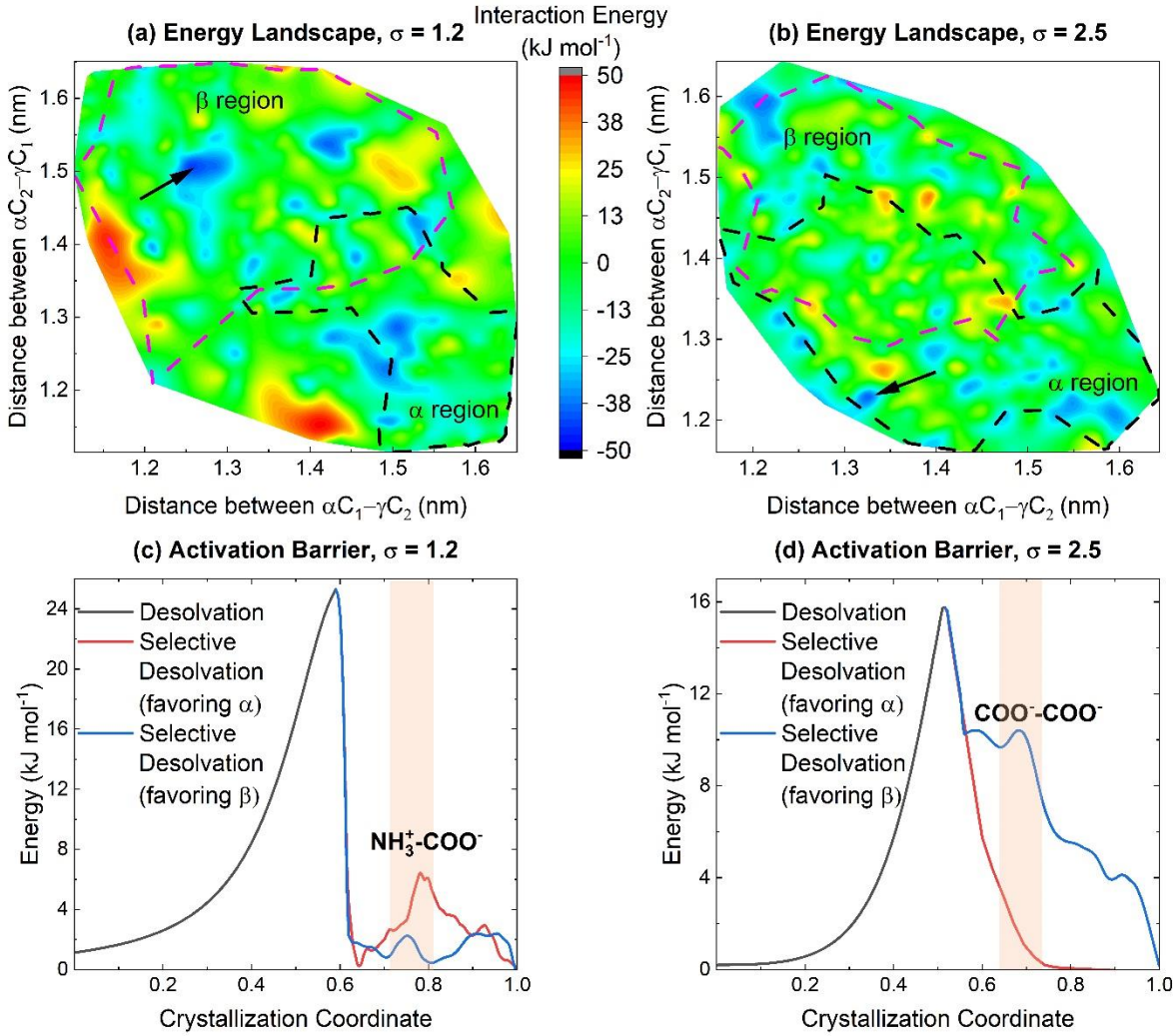

Figure 4: Interaction energy landscape of the two GLU molecules after the first transition from fully solvated to partially desolvated states. Interaction energy profiles for various possible orientations of partially desolvated GLU molecules were obtained at the supersaturation ratio of (a) σ = 1.2, and (b) σ = 2.5. The black arrows indicate the location of global minimum in the energy landscapes, the black dotted curve shows the α-polymorph similarity region, and the magenta dotted curve shows the β-polymorph similarity region. Potential energy profiles obtained from umbrella sampling at (c) σ = 1.2 and (d) σ = 2.5. The solid black curve in (c) and (d) were obtained from the potential of mean force approach and represent the first step of nucleation where fully solvated molecules attain a partially desolvated state to form an unordered dense phase. The blue and red curves show the potential energy profiles obtained by the umbrella sampling method for

each polymorph. The shaded region in (c) and (d) shows the additional activation barriers arising due to group-specific interaction in the second step of nucleation.

The results obtained using the energy landscape and umbrella sampling techniques are further validated by performing crystallization of GLU molecules in a continuous-flow microfluidic setup.(28, 29) The crystallization was performed at supersaturation ratios ranging from 1.3 to 4.7. The two polymorphs of the GLU crystals can be distinguished using the morphology where the α polymorph has plate-like morphology, and the β polymorph has needle-like morphology. The percentage of β form was obtained by using an image analysis program, and the results are shown in **Figure 5**. At low supersaturation values of 1.3 and 1.6 (**Figures 5a and 5b**), only β polymorph is crystallized. However, as the supersaturation increases (**Figures 5c-5f**), the percentage of β polymorph reduces significantly to the extent that no β polymorph is observed at high supersaturation. The percentage of β polymorph is shown in **Figure 5g**. The activation barriers shown in **Figures 4c-4d** were used to perform a kinetic Monte-Carlo (kMC) simulation to predict the percentage of β polymorph at the supersaturation ratios of 1.2, 2, and 2.5 (refer to **Section S4** and **Figure S14** of the SI). Results obtained from the activation barrier predict a high percentage of β polymorph at low supersaturation and reduction of the percentage of β polymorph as a function of supersaturation. These predictions are in good agreement with the experiments.

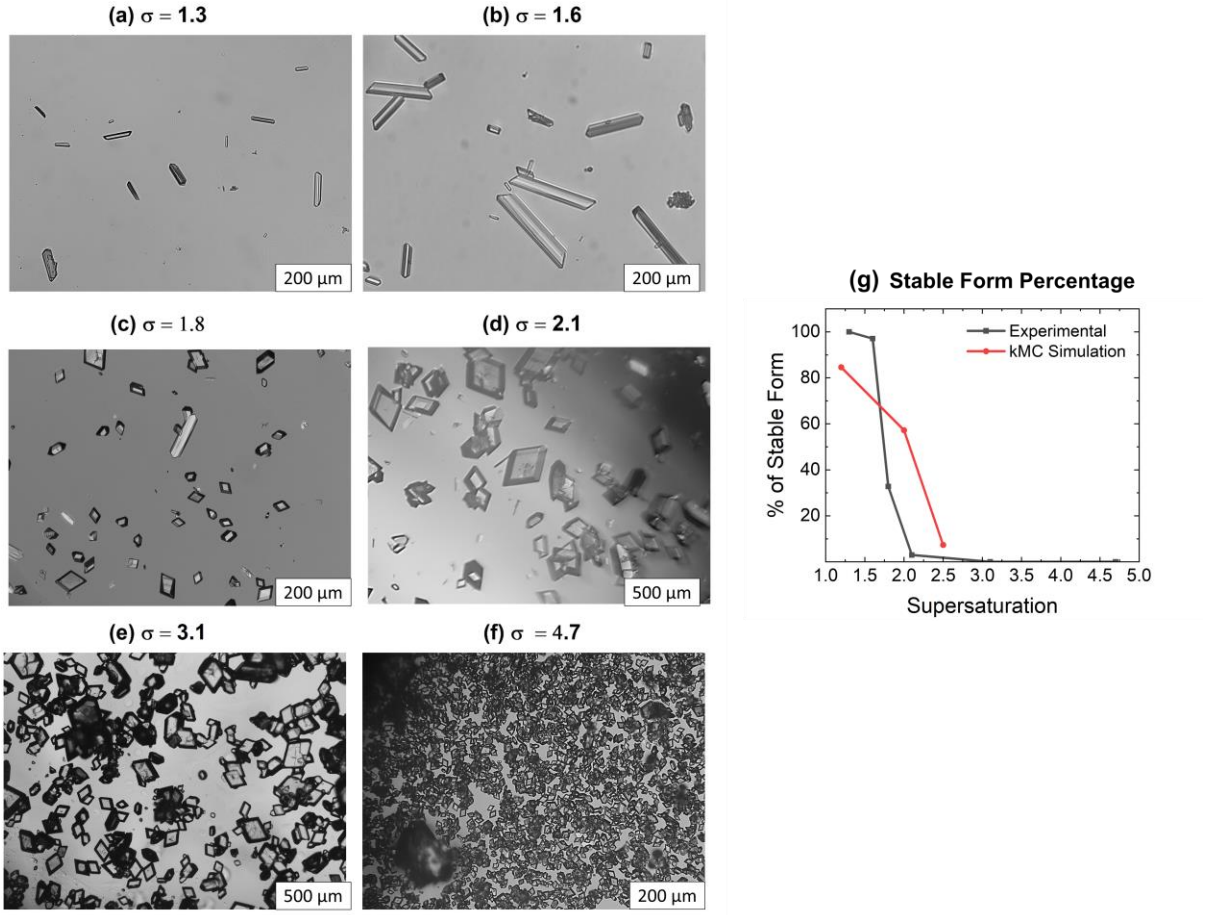

Figure 5: Continuous crystallization of GLU in a microfluidic device and percentage of stable (β) polymorph as a function of supersaturation. (a) – (f) show the snapshot of GLU crystals as a function of supersaturation. (a) σ = 1.3 (b) σ = 1.6 (c) σ = 1.8 (d) σ = 2.1 (e) σ = 3.1 (f) σ = 4.7. The α polymorph has plate-like morphology while the β polymorph has needle-like morphology, which is then used to calculate the percentage of β polymorph. (g) Percentage of stable β polymorph observed experimentally compared with the corresponding values predicted using kinetic Monte Carlo simulations.

Conclusion

This article provides molecular insights into crystal structure formation in a framework of a two-step nucleation mechanism. The molecular simulations of the glutamic acid (GLU) molecules uncover the dynamics of sequential desolvation around the functional groups during crystallization. The partially charged zwitterionic functional groups of GLU molecules contribute significantly towards the uneven distribution of water molecules around the GLU. The NH_3^+ functional group has the highest affinity towards the water and prevents the formation of α polymorph at low supersaturation. The highly desolvated COO^- functional group causes strong repulsive electrostatic interactions, which causes an additional activation barrier in the formation

of β polymorph at high supersaturation. These are the direct effects of desolvation on crystal structure formation, which have not been accounted for so far in the literature.

The results shown in this article have unified two disjointed approaches – two-step nucleation theory and crystal structure prediction (CSP) techniques – in the field of crystallization. Crystallization, mainly a purification process, consists only of the self-assembly of solute molecules in a supersaturated environment. Yet, the highly stochastic nature and the strong intermolecular interactions driven by supersaturation causes variability in the outcome of crystallization. Such variability was previously attributed only to the lattice energy of various crystal structures using CSP techniques. However, here we have shown that the outcome of crystallization is strongly dependent upon the kinetics of solute-solvent interactions as well as the energetics of crystal packing.

The multiple minima, as seen on the activation barrier diagram and the energy landscape, corroborates with the non-classical two-step nucleation mechanism indicating the formation of dense phase before the formation of crystalline product. Here we find that the first step is the partial desolvation of solute to form an unordered dense phase, and the second step is the selective desolvation of functional groups to form specific polymorphs. Simulations depict that the kinetics of solute-solvent interactions direct the packing of molecules in the crystal structure. Overall, the results point toward the need for controlling solvation dynamics to steer crystal structure formation.

Methods

Computational:

The GROMACS code was used to set up a dodecahedron box of 216.48 nm^3 which was used to create simulation boxes for supersaturation of 1.2, 1.5, 2, and 2.5. The experimental solubility of glutamic acid was used as the basis to decide the number of glutamic acid molecules and water molecules inside the simulation boxes. Optimized Potentials for Liquid Simulations – All Atom (OPLS-AA) force field was used to perform molecular dynamics simulations. A simple point charge extended (SPCE) water model was used in all the simulation boxes. Periodic boundary conditions were applied in all three directions. The cut-off radius of 1 nm was used for van der Waals interaction. The potential mesh Ewald summation method was used long-range electrostatic interactions. The equilibration simulations were performed on isothermal and isobaric ensembles for one ns each. The production run for five ns was performed using an isobaric ensemble. The data were obtained at every one ps, resulting in 5000 data points for each analysis. The built-in trajectory analysis tools of GROMACS code were used to obtain group function-specific RDFs. The package named “Trajectory Analyzer and Visualizer” (Travis) was used to obtain all the spatial distribution functions shown in the article. For SDF calculations, the simulation box was binned into 100 points in each direction.

Experimental:

In this study, cooling crystallization of L-Glutamic acid in water at different concentrations was done. The single crystal data for both polymorphs is given in **Table S2** of the SI. Saturated samples

of L-Glutamic acid in water were prepared at different temperatures and then cooled down to the desired temperature to target different values of supersaturation. Cooling crystallization was performed using a 3D printed microfluidic device. The 3D design of the device was initially made using SolidWorks and then fabricated with a FORM 2, a 3D printer. The microfluidic device includes a cylindrical chamber that has four tangential inlets connected to it. The chamber has an outlet on the top and is surrounded by a jacketed area. The cooling liquid goes around the chamber and decreases the temperature of the streams that enter the chambers. The height of the jacketed area is kept at a constant ratio to decrease the temperature gradient within the chamber and reach a homogenous temperature lower than the inlets. In these experiments, a mixture of ice and water was used for 0℃ of the coolant stream. A syringe pump was used to pump the saturated streams into the system. Syringe heaters were connected to the syringes before filling them up to maintain the temperature. The setup was kept under an optical microscope (Olympus BX53M, Olympus America Inc.), and optical images were taken from each sample for comparing the form percentages.

Acknowledgments

This material is based on the work performed at the Materials and Systems Engineering Laboratory at the University of Illinois at Chicago (UIC). M.R.S. acknowledges funding support from UIC and the US National Science Foundation (NSF, EFRI 2132022).

Competing Interests:

The authors declare that there are no competing interests.

Author Contributions:

M.R.S. conceptualized research; M.R.S and A.V.D. designed methodology, AV.D., and P. K. R. P., performed theoretical investigation, P.C., performed experimental investigation; A.V.D., P.C., P.K.R.P., and M.R.S. performed validation; M.R.S., A.V.D., and P.C. wrote the original draft., M.R.S., A.V.D., P.K.R.P performed review and editing of the original draft.

Data Availability:

All data generated or analysed during this study are included in this published article (and its SI files).

References:

1. P. G. Vekilov, The two-step mechanism of nucleation of crystals in solution. *Nanoscale* **2**, 2346-2357 (2010).

2. R. P. Sear, Quantitative studies of crystal nucleation at constant supersaturation: experimental data and models. *Crystengcomm* **16**, 6506-6522 (2014).
3. A. Haji-Akbari, P. G. Debenedetti, Direct calculation of ice homogeneous nucleation rate for a molecular model of water. *Proceedings of the National Academy of Sciences* **112**, 10582-10588 (2015).
4. L. Zhang, W. Ren, A. Samanta, Q. Du, Recent developments in computational modelling of nucleation in phase transformations. *npj Computational Materials* **2**, 16003 (2016).
5. D. Erdemir, A. Y. Lee, A. S. Myerson, Nucleation of Crystals from Solution: Classical and Two-Step Models. *Accounts of Chemical Research* **42**, 621-629 (2009).
6. R. M. Stratt, M. Maroncelli, Nonreactive dynamics in solution: The emerging molecular view of solvation dynamics and vibrational relaxation. *J Phys Chem-Us* **100**, 12981-12996 (1996).
7. M. Maroncelli, Computer-Simulations of Solvation Dynamics in Acetonitrile. *J Chem Phys* **94**, 2084-2103 (1991).
8. B. Bagchi, B. Jana, Solvation dynamics in dipolar liquids. *Chem Soc Rev* **39**, 1936-1954 (2010).
9. R. Jimenez, G. R. Fleming, P. V. Kumar, M. Maroncelli, Femtosecond Solvation Dynamics of Water. *Nature* **369**, 471-473 (1994).
10. F. O. Raineri, H. Resat, B. C. Perng, F. Hirata, H. L. Friedman, A molecular theory of solvation dynamics. *The Journal of Chemical Physics* **100**, 1477-1491 (1994).
11. R. Rey, J. T. Hynes, Solvation Dynamics in Liquid Water. 1. Ultrafast Energy Fluxes. *J Phys Chem B* **119**, 7558-7570 (2015).
12. R. Rey, J. T. Hynes, Solvation Dynamics in Water: 2. Energy Fluxes on Excited- and Ground-State Surfaces. *J Phys Chem B* **120**, 11287-11297 (2016).
13. R. Rey, J. T. Hynes, Solvation Dynamics in Liquid Water. III. Energy Fluxes and Structural Changes. *J Phys Chem B* **121**, 1377-1385 (2017).
14. R. Vangara, F. v. Swol, D. N. Petsev, Ionic solvation and solvent-solvent interaction effects on the charge and potential distributions in electric double layers. *The Journal of Chemical Physics* **147**, 214704 (2017).
15. J. N. Dahanayake *et al.*, Protein Solvent Shell Structure Provides Rapid Analysis of Hydration Dynamics. *Journal of Chemical Information and Modeling* **59**, 2407-2422 (2019).
16. O. Dopfer, M. Fujii, Probing Solvation Dynamics around Aromatic and Biological Review Molecules at the Single-Molecular Level. *Chemical Reviews* **116**, 5432-5463 (2016).
17. M. N. Joswiak, M. F. Doherty, B. Peters, Ion dissolution mechanism and kinetics at kink sites on NaCl surfaces. *P Natl Acad Sci USA* **115**, 656-661 (2018).
18. A. S. Myerson, *Handbook of industrial crystallization* (Butterworth-Heinemann, 2002).
19. D. Kashchiev, P. G. Vekilov, A. B. Kolomeisky, Kinetics of two-step nucleation of crystals. *The Journal of chemical physics* **122**, 244706 (2005).
20. M. Kowacz, M. Prieto, A. Putnis, Kinetics of crystal nucleation in ionic solutions: Electrostatics and hydration forces. *Geochimica Et Cosmochimica Acta* **74**, 469-481 (2010).
21. S. L. Price, Computed crystal energy landscapes for understanding and predicting organic crystal structures and polymorphism. *Accounts of Chemical Research* **42**, 117-126 (2009).
22. D. A. Bardwell *et al.*, Towards crystal structure prediction of complex organic compounds - a report on the fifth blind test. *Acta Crystallogr B* **67**, 535-551 (2011).

23. A. M. Reilly *et al.*, Report on the sixth blind test of organic crystal structure prediction methods. *Acta Crystallogr B* **72**, 439-459 (2016).
24. R. M. Bhardwaj *et al.*, A Prolific Solvate Former, Galunisertib, under the Pressure of Crystal Structure Prediction, Produces Ten Diverse Polymorphs. *Journal of the American Chemical Society* **141**, 13887-13897 (2019).
25. A. V. Dighe, M. R. Singh, Solvent fluctuations in the solvation shell determine the activation barrier for crystal growth rates. *Proc Natl Acad Sci U S A* **116**, 23954-23959 (2019).
26. M. T. Ruggiero, J. Sibik, J. A. Zeitler, T. M. Korter, Examination of L-Glutamic Acid Polymorphs by Solid-State Density Functional Theory and Terahertz Spectroscopy. *J Phys Chem A* **120**, 7490-7495 (2016).
27. E. Shustorovich, Energetics of metal-surface reactions: back-of-the-envelope theoretical modeling. *Journal of Molecular Catalysis* **54**, 301-311 (1989).
28. P. Coliaie *et al.*, Advanced continuous-flow microfluidic device for parallel screening of crystal polymorphs, morphology, and kinetics at controlled supersaturation. *Lab Chip* **21**, 2333-2342 (2021).
29. P. Coliaie, M. S. Kelkar, N. K. Nere, M. R. Singh, Continuous-flow, well-mixed, microfluidic crystallization device for screening of polymorphs, morphology, and crystallization kinetics at controlled supersaturation. *Lab Chip* **19**, 2373-2382 (2019).